J|A|C|S ARTICLES

Published on Web 02/05/2010

Pillared MFI Zeolite Nanosheets of a Single-Unit-Cell Thickness

Kyungsu Na,[†] Minkee Choi,[†] Woojin Park,[†] Yasuhiro Sakamoto,[‡,§] Osamu Terasaki,[‡,||] and Ryong Ryoo*[,†,⊥]

Center for Functional Nanomaterials, Department of Chemistry, Graduate School of EEWS (WCU), Graduate School of Nanoscience and Technology (WCU), KAIST, Daejeon 305-701, Korea, Structural Chemistry, Arrhenius Laboratory, Stockholm University, 10691 Stockholm, Sweden, and Nanoscience and Nanotechnology Research Center, Osaka Prefecture University, Sakai 599-8570, Japan

Received October 2, 2009; E-mail: rryoo@kaist.ac.kr

Abstract: Zeolite MFI nanosheets of 2-nm thickness have been hydrothermally synthesized via cooperative assembly between silica and an organic surfactant, which is functionalized with a diquaternary ammonium group. The zeolite nanosheets have been further assembled into their ordered multilamellar mesostructure through hydrophobic interactions between the surfactant tails located outside the zeolite nanosheet. This assembly process involves successive transformations from an initially hexagonal mesophase to a multilamellar mesophase without crystallinity and then to a lamellar mesophase with a crystalline zeolite framework. The mesopore volume in the interlamellar space could be retained by supporting the zeolite nanosheets with silica pillars, as in pillared clays, even after surfactant removal by calcination. The mesopore diameters could be controlled according to the surfactant tail lengths. Due to the interlamellar structural coherence, the hierarchically mesoporous/microporous zeolite could exhibit small-angle X-ray diffraction peaks up to the fourth-order reflections corresponding to the interlayer distance. In addition, an Ar adsorption analysis and transmission electron microscopic investigation indicated that the pillars were highly likely to be built with an MFI structure. The present approach using a zeolite structure-directing functional group contained in a surfactant would be suitable for the synthesis of other related nanomorphous zeolites in the future.

Introduction

Many types of inorganic porous materials can be synthesized through a process whereby an inorganic framework is assembled via interactions with an organic pore-generating species (porogen) in solution. Zeolite is a typical example of a microporous (<2 nm) material synthesized in this manner. The crystalline aluminosilicate framework of zeolite is generated by using an organic amine as a molecular porogen.[1,2] Ordered mesoporous molecular sieves like MCM-41 and SBA-15 can also be synthesized using an organic porogen, but mesopores (2−50 nm) are generated by a supramolecular assembly of the porogen molecules.[3,4] These porous materials are obtained as a metastable phase, since the pore generation is a thermodynamically less favorable process than the formation of a fully condensed phase. The synthesis process must be controlled very delicately using both the thermodynamic and kinetic driving forces for the framework formation. When micropores and mesopores are to be simultaneously generated in a hierarchical way, the synthesis becomes more difficult to control. When two types of porogen are used simultaneously in a single material synthesis, the result tends to be a solely microporous product, a solely mesoporous material, or a mixture thereof.[5]

Synthesis of ordered and hierarchically porous zeolites by self-assembly is a major challenge in chemical sciences. The synergetic combination of an MCM-41-like ordered mesostructure with a zeolite-like crystalline microporous feature can accommodate maximum functions in a limited volume and also realize high diffusion efficiencies. Microporous zeolite materials with an MFI structure were synthesized in a form with inter- and intracrystalline mesopores.[6,7] The hierarchically meso-/microporous zeolites exhibited remarkably improved catalytic lifetimes as compared to a solely microporous zeolite.[8] However, structural order in the mesopore arrangement was not realized in these materials. An MFI zeolite exhibiting a three-dimensionally ordered mesoporous (3DOM) feature was reported by Fan

[†] Department of Chemistry, KAIST.
[‡] Stockholm University.
[§] Osaka Prefecture University.
[||] Graduate School of EEWS (WCU), KAIST.
[⊥] Graduate School of Nanoscience and Technology (WCU), KAIST.

(1) Cundy, C. S.; Cox, P. A. *Chem. Rev.* **2003**, *103*, 663–701.
(2) Cundy, C. S.; Cox, P. A. *Microporous Mesoporous Mater.* **2005**, *82*, 1–78.
(3) Kresge, C. T.; Leonowicz, M. E.; Roth, W. J.; Vartuli, J. C.; Beck, J. S. *Nature* **1992**, *359*, 710–712.
(4) Zhao, D.; Huo, Q.; Melosh, N.; Frederickson, G. H.; Chmelka, B. F.; Stucky, G. D. *Science* **1998**, *279*, 548–552.
(5) Karlsson, A.; Stöcker, M.; Schmidt, R. *Microporous Mesoporous Mater.* **1999**, *27*, 181–192.
(6) Jacobsen, C. J. H.; Madsen, C.; Houzvicka, J.; Schmidt, I.; Carlsson, A. *J. Am. Chem. Soc.* **2000**, *122*, 7116–7117.
(7) Choi, M.; Cho, H. S.; Srivastava, R.; Venkatesan, C.; Choi, D.-H.; Ryoo, R. *Nat. Mater.* **2006**, *5*, 718–723.
(8) Srivastava, R.; Choi, M.; Ryoo, R. *Chem. Commun.* **2006**, *43*, 4489–4491.

et al.,[9] but the synthesis reaction had to be performed in a 3DOM-type carbon template.

In a previous work, we reported the development of ultrathin MFI zeolite nanosheets, which corresponded to only a single-unit-cell thickness (2.0 nm along *b*-axis).[10] The zeolite nanosheets were hydrothermally synthesized using an organic surfactant functionalized with a diquaternary ammonium group in the head, i.e., $C_{22}H_{45}-N^+(CH_3)_2-C_6H_{12}-N^+(CH_3)_2-C_6H_{13}$. The role of the headgroup was a zeolite-structure directing agent (SDA), while the hydrophobic interaction between the C_{22}-alkyl tails led to supramolecular organization of the surfactant molecules into a lamellar structure. Depending on the synthesis conditions, the zeolite nanosheets were self-organized into a disordered unilamellar assembly or an ordered multilamellar stack. The former retained a high mesoporosity upon removal of the surfactant through calcination, and the mesopores were irregular. Nonetheless, due to the hierarchically mesoporous and microporous structure, the zeolite exhibited a remarkably improved catalytic lifetime for catalytic conversion of methanol to gasoline, compared to an ordinary MFI zeolite. In the case of the multilamellar zeolite, although the as-synthesized sample exhibited an excellent structural correlation between adjacent layers, the structural order was lost upon calcination. The zeolite was not fully mesoporous due to interlayer condensation upon removal of the SDA. No other mesostructures have yet been obtained thus far using a zeolite-SDA-functionalized surfactant. It still remains as a challenge to use one kind of porogen molecule to generate two types of ordered micro- and mesoporous systems simultaneously.

Pillaring is a useful process to intercalate guest species between interlayer spacings of layered materials.[11] Many clay materials have a layered sheetlike structure. The interlayer spacings can be supported by pillars after being expanded through a suitable intercalation process. The pillared clays may possess pores with very uniform thickness between adjacent layers when the pillars are rigid and spaced sufficiently.[12,13] Pillaring with thermally stable inorganic species can preserve the ordered structure of the layered materials and also introduce chemical functions in addition to the intrinsic features of host materials.[11,14−17] Some zeolites such as MWW and FER can be synthesized through layered precursors before being fully converted to 3D ordered microporous frameworks.[14−17] These zeolite precursors with a 2D structure can be pillared with silica after being expanded with an organic swelling agent. In principle, pillaring can impart the microporous zeolites with uniform mesopores.[11] New features such as high surface area and facile accessibility for bulky molecules can be developed due to the mesoporosity. The mesopore diameters can be controlled through a suitable choice of guest species,[11] but precise control has not yet been demonstrated for zeolites under experimental conditions using ultrasonic waves. Furthermore, zeolite pillaring has been limited to the layered zeolites, excluding most zeolites with 3D structure.

Herein, we report on pillaring of a multilamellar MFI zeolite that we synthesized using $C_{22}H_{45}-N^+(CH_3)_2-C_6H_{12}-N^+(CH_3)_2-C_6H_{13}$ as a SDA. Pillaring was carried out with tetraethoxysilane (TEOS) prior to SDA removal. The pillared MFI zeolite nanosheets possessed mesopores with very uniform diameters in the interlamellar space. The mesopore diameters could be precisely controlled according to the surfactant tail lengths. Due to the interlamellar structural coherence, the hierarchically mesoporous/microporous zeolite exhibited small-angle X-ray diffraction peaks up to the fourth-order reflections corresponding to the interlayer distance. Among zeolites with 3D structure, this is the first material exhibiting two kinds of structural orders simultaneously in both mesoporous and microporous regimes. Ar adsorption analysis and transmission electron microscopic investigation indicate that the pillars are highly likely to be built with an MFI structure. We also report on the details of the multilamellar zeolite synthesis which were not reported previously. The present paper discusses synthesis conditions for multilamellar MFI zeolite nanosheets, effects of Al incorporation, control of interlamellar spacings, and the transformation from noncrystalline mesoporous silica to the crystalline zeolite nanosheets during hydrothermal synthesis.

Experimental Section

Preparation of SDAs. The zeolite-SDA-functional surfactant, $[C_{22}H_{45}-N^+(CH_3)_2-C_6H_{12}-N^+(CH_3)_2-C_6H_{13}]Br_2$, was synthesized in two steps following the procedure of Choi et al.[10] In a typical synthesis, 3.9 g (0.01 mol) of 1-bromodocosane (TCI) and 17.2 g (0.1 mol) of *N,N,N′,N′*-tetramethyl-1,6-diaminohexane (Aldrich) were dissolved in 100 mL of acetonitrile/toluene mixture (1:1 v/v) and reacted under magnetic stirring at 60 °C for 10 h. After cooling to room temperature, the precipitated product was $[C_{22}H_{45}-N^+(CH_3)_2-C_6H_{12}-N(CH_3)_2]Br$. This compound, designated as $C_{22-6-0}Br$, was filtered, washed with cold diethyl ether, and dried in a vacuum oven at 50 °C for removal of the organic solvent. Then 5.6 g (0.01 mol) of $C_{22-6-0}Br$ and 2.5 g (0.02 mol) of 1-bromohexane (Aldrich) were dissolved in 30 mL of acetonitrile and refluxed for 10 h. After cooling to room temperature, the precipitated product was filtered, washed with cold diethyl ether, and dried in a vacuum oven at 50 °C.

The product was identified as $[C_{22}H_{45}-N^+(CH_3)_2-C_6H_{12}-N^+(CH_3)_2-C_6H_{13}]Br_2$ by ^1H NMR, which was taken from a $CDCl_3$ solution using a Bruker Avance instrument. This compound is denoted as $C_{22-6-6}Br_2$. Two more surfactants with a C_{22}-alkyl chain were synthesized following the same procedure used for $C_{22-6-6}Br_2$, except for the substitution of 1-bromohexane with 1-bromopropane and 1-bromooctane (Aldrich). These surfactants are denoted as $C_{22-6-3}Br_2$ and $C_{22-6-8}Br_2$, respectively. Surfactants with shorter tails than the C_{22}-alkyl chain were also obtained by the synthesis procedure described above, using suitable bromoalkanes. These are $C_{12-6-3}Br_2$, $C_{16-6-6}Br_2$, $C_{18-6-6}Br_2$, and $C_{20-6-6}Br_2$.

The synthesized surfactants were used as zeolite-SDAs in the bromide forms or after exchanging Br^- to OH^-. The ion exchange to OH^- was performed by passing an aqueous solution twice through a column packed with anion exchange resin (MTO−Dowex SBR LCNG OH form, Supelco). The surfactant content after the ion exchange treatment was 10−20 wt % in water.

Synthesis of Zeolite Nanosheets. In principle, the hydrothermal synthesis of MFI zeolite nanosheets was performed by following the method of Choi et al.[10] Various zeolite-SDA-functional

(9) Fan, W.; et al. *Nat. Mater.* **2008**, *7*, 984–991.
(10) Choi, M.; Na, K.; Kim, J.; Sakamoto, Y.; Terasaki, O.; Ryoo, R. *Nature* **2009**, *461*, 246–249.
(11) Tsapatsis, M.; Maheshwari, S. *Angew. Chem., Int. Ed.* **2008**, *47*, 4262–4263.
(12) Behrens, M.; Riemenschneider, O.; Bensch, W.; Indris, S.; Wilkening, M.; Heitjans, P. *Chem. Mater.* **2006**, *18*, 1569–1576.
(13) Whittingham, M. S.; Song, Y. N.; Lutta, S.; Zavalij, P. Y.; Chernova, N. A. *J. Mater. Chem.* **2005**, *15*, 3362–3379.
(14) Roth, W. J.; Kresge, C. T.; Vartuli, J. C.; Leonowicz, M. E.; Fung, A. S.; McCullen, S. B. *Stud. Surf. Sci. Catal.* **1995**, *94*, 301–308.
(15) Corma, A.; Diaz, U.; Domine, M. E.; Fornés, V. *Angew. Chem., Int. Ed.* **2000**, *39*, 1499–1501.
(16) Maheshwari, S.; Jordan, E.; Kumar, S.; Bates, F. S.; Penn, R. L.; Shantz, D. F.; Tsapatsis, M. *J. Am. Chem. Soc.* **2008**, *130*, 1507–1516.
(17) Maheshwari, S.; Jordan, E.; Kumar, S.; Bates, F. S.; Penn, R. L.; Shantz, D. F.; Tsapatsis, M. *Angew. Chem., Int. Ed.* **2008**, *47*, 552–555.

surfactants were used as synthesized above. The detailed synthetic parameters were varied. The starting molar composition for the multilamellar MFI zeolite nanosheets was varied within x Al_2O_3:30 Na_2O:100 SiO_2:10 SDA:18 H_2SO_4:y ethanol:4000 H_2O. The silica source was varied in TEOS (TCI), water glass (an aqueous solution of sodium silicate, Si/Na = 1.75, 29 wt % SiO_2), and fumed silica (Aerosil, Degussa). The alumina source was aluminum sulfate [$Al_2(SO_4)_3 \cdot 18H_2O$, Aldrich], with variation of x = 0, 0.33, 0.5, 1, 2, and 3.3. Various organic SDAs as synthesized above were tested in this composition. The number of ethanol moles (y) was varied as 400, 800, and 1600.

In a typical synthesis, a highly basic solution was obtained by dissolving NaOH, ethanol, and SDA in distilled water. This solution was added with an acidic aqueous solution of $Al_2(SO_4)_3 \cdot 18H_2O$ and H_2SO_4. The acidic solution was added dropwise under vigorous stirring. Agitation was continued for 1 h at 60 °C. After cooling to room temperature, a silica source was quickly added into this solution under vigorous mixing using an electric mixer or a magnetic stirrer. After continuous mixing for 1 h at 60 °C, the resultant gel was transferred into a Teflon-lined stainless-steel autoclave. This autoclave was heated at 150 °C for 5−20 d under tumbling in an oven (60 rpm). Multilamellar or unilamellar MFI zeolites were produced during the autoclave heating, depending on the details of the synthesis conditions. The zeolite products were filtered and dried at 120 °C. Some of the multilamellar zeolite samples were used for pillaring experiments. The pillaring procedure is described in the following subsection. Other samples were calcined at 550 °C for 4 h in air to remove the SDA. The multilamellar samples after calcinations are designated as C_n-MFI according to the alkyl group of the SDA (i.e., 12, 16, 18, 20, or 22), while the pillared samples are designated as P-C_n-MFI.

Other Porous Silica or Aluminosilicate Samples. Conventional MFI zeolite was purchased from Zeolyst (sample codes CBV 8014, Si/Al = 41). This sample was designated as conv-MFI, and used as a conventional sample. An MCM-41 sample was synthesized according to a method reported in the literature.[18] For Al incorporation on MCM-41, 1.00 g of calcined MCM-41 was stirred in an ethanol solution containing 0.045 g of $AlCl_3$ for 3 h.[19] After the ethanol evaporated, the MCM-41 was calcined at 550 °C for 4 h in air. This sample is designated as Al-MCM-41. The inductively coupled plasma (ICP) analysis indicated that the Si/Al ratios of conv-MFI and Al-MCM-41 were 41 and 46, respectively.

Pillaring of Multilamellar MFI Nanosheets. Pillaring was carried out with TEOS, following the method of the Tsapatsis group for pillaring of MWW zeolite,[16] except for the preswelling step. This pillaring process infiltrates TEOS into the surfactant region between adjacent zeolite nanosheets and converts it to silica pillars through hydrolysis. In a typical synthesis, 1.0 g of as-synthesized multilamellar sample was stirred in 5.0 g of TEOS for 12 h at room temperature. The zeolite sample after filtering was dried at 35 °C for 12 h, to remove the residual TEOS that should be weakly bound on the external surface. A 1.0 g portion of the resultant sample was stirred in 10.0 g of distilled water at 90 °C for 12 h, in order to hydrolyze TEOS. The sample was filtered, washed with distilled water, dried at 120 °C, and calcined at 550 °C for 4 h in air. ICP analysis indicated that the Si/Al ratio of the C_{22}-MFI sample was increased from 49 to 57 due to intercalation by the additional silica source. The same treatment of C_{16}-MFI increased the Si/Al ratio from 45 to 55.

Characterization. Powder X-ray diffraction (XRD) patterns were obtained using a Rigaku Multiflex diffractometer equipped with Cu Kα radiation (40 kV, 30 mA). Scanning electron micrograph (SEM) images were taken with a Hitachi S-4800 and a JEOL JSM-7401F at a low landing energy (0.3−0.6 kV, in gentle-beam mode) without crushing or a metal coating. Transmission electron microscope (TEM) images were taken with a JEOL JEM-3010 with an accelerating voltage of 300 kV (Cs = 0.6 mm, point resolution 0.17 nm).

Ar adsorption isotherms were measured at liquid Ar temperature with an ASAP2020 Micromeritics volumetric adsorption analyzer. Before measurements, all samples were degassed under vacuum for 12 h at 300 °C. The Brunauer−Emmett−Teller (BET) equation was used to calculate the BET specific surface area from the adsorption data obtained at P/P_0 between 0.1 and 0.3. Nonlocal density functional theory (NLDFT) analyses were carried out to characterize pore volume and size. For the analyses, the kernel of NLDFT equilibrium capillary condensation isotherms of Ar at 87 K on silica was selected for the model isotherms (using adsorption branch, and assuming cylindrical pores).

For NH_3 temperature-programmed desorption (TPD) measurements and IR analyses, all samples were NH_4^+-ion-exchanged with a 1 M NH_4NO_3 aqueous solution (NH_4NO_3/Al in the samples = 10).[7] The ion exchange process was repeated twice. After filtering and drying, the NH_4^+-ion-exchanged samples were calcined in air at 550 °C to be converted to the H^+-form. For the NH_3-TPD measurement, 50 mg of each sample was put into a quartz reactor and degassed for 3 h at 550 °C under a He flow (30 mL/min).[7] After cooling to room temperature, NH_3 gas was flowed into the quartz reactor to be adsorbed on the acid sites of the samples for 1 h with a flow rate of 30 mL/min. Subsequently, free and weakly adsorbed NH_3 species were removed by flowing He for 1 h at 100 °C. TPD profiles were then measured by using a thermal conductivity detector, with a continuous temperature increase (10 °C/min) under He flow (30 mL/min).

For IR measurement, all samples were pressed to produce self-supporting wafers (ca. 12 mg/cm^2) without binding agents.[20] The samples were subsequently degassed at 500 °C for 2 h in an in situ IR cell. After cooling down to room temperature, IR spectra were collected by using an FT-IR spectrometer (Bruker Vector 33) at room temperature with 40 scans and 4 cm^{-1} resolution for each spectrum. For measurement of external acidity, a bulky amine precursor, 2,6-di-*tert*-butylpyridine (2,6-DTBPy), was adsorbed on the degassed self-supporting wafer in an in situ IR cell for 1 h at 150 °C.[20] The physisorbed and weakly bound species were then desorbed for 1 h under vacuum at the same temperature. After cooling down to room temperature, IR spectra were collected by using the same instrument at the same conditions noted above.

Results and Discussion

Synthesis Conditions for Multilamellar MFI Zeolite Nanosheets. Synthesis of MFI zeolite nanosheets was tried under various hydrothermal conditions, using various organic surfactants as SDAs. A very successful result was obtained with $C_{22-6-6}Br_2$ at 150 °C, as reported by Choi et al.[10] It was also possible to synthesize zeolite nanosheets at 130 °C, but the zeolite crystallization required a much longer reaction time than that at 150 °C. Some of the representative synthesis conditions using $C_{22-6-6}Br_2$ at 150 °C are given in Table 1. Among them, condition a corresponds precisely with that used by Choi et al. for the synthesis of ordered multilamellar nanosheets.[10] The "400 mol of EtOH" in the synthesis composition is from the hydrolysis of TEOS.

Figure 1 shows as-synthesized XRD patterns for the products obtained under the conditions listed in Table 1. Note that the XRD data in trace a exhibits two low-angle peaks indexed as (1) and (3), whereas the high-angle XRD peaks are characteristic of a crystalline MFI zeolite. The low-angle peaks can be assigned to the first- and third-order reflections corresponding to interlamellar structural correlation in the multilamellar MFI

(18) Ryoo, R.; Ko, C. H.; Park, I.-S. *Chem. Commun.* **1999**, *141*, 3–1414.
(19) Jun, S.; Ryoo, R. *J. Catal.* **2000**, *195*, 237–243.
(20) Corma, A.; Fornés, V.; Forni, L.; Márquez, F.; Martínez-Triguero, J.; Moscotti, D. *J. Catal.* **1998**, *179*, 451–458.

Table 1. Synthesis Conditions[a] and Morphologies of the Resultant MFI Zeolite

condition (and label for XRD in Figure 1)	silica source	*y* (EtOH)	reaction time (d)	zeolite product
a	TEOS	400	4	multilamellar MFI nanosheets
b	TEOS	800	7	disordered MFI nanosheets and bulk
c	TEOS	1600	7	disordered MFI nanosheets and bulk
d	water glass[b]	0	6	multilamellar MFI nanosheets
e	water glass	400	4	multilamellar MFI nanosheets
f	fumed silica	0	7	disordered MFI nanosheets and bulk
g	fumed silica	400	7	disordered MFI nanosheets and bulk

[a] All syntheses were performed with the same starting compositions of 100 SiO_2:1 Al_2O_3:30 Na_2O:10 $C_{22-6-6}Br_2$:18 H_2SO_4:*y* EtOH:4000 H_2O at 150 °C in tumbled autoclaves. [b] An aqueous solution of sodium silicate containing 29 wt % SiO_2 (Si/Na = 1.75).

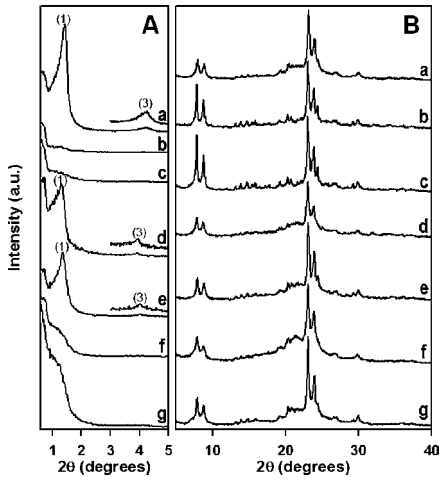

Figure 1. Low-angle (A) and high-angle (B) XRD patterns for as-synthesized MFI zeolite products, which were synthesized with $C_{22-6-6}Br_2$. The labels a−g correspond to synthesis conditions a−g given in Table 1, respectively.

zeolite. The first-order reflection is observed at $2\theta = 1.45°$ ($d_{(1)} = 6.1$ nm). After subtracting the nanosheet thickness (2.0 nm) from 6.1 nm, the remainder (4.1 nm) is the thickness of the surfactant layer located between the two adjacent nanosheets. The second-order reflection is missing due to an accidental extinction, which can be explained by the coincidence between the thickness of a single MFI nanosheet and one-half of the surfactant-layer thickness.[21] The presence of the third-order reflection indicates that the long-range structural order is excellent. Thus, a highly ordered multilamellar structure was obtained after 4-d hydrothermal reaction under synthesis condition a in Table 1.

When the reaction mixture was further heated in an autoclave beyond 4 d, the high-angle XRD peaks did not change substantially. However, the small-angle peaks became further narrower and increased in intensity. This indicates that the multilamellar structural order increased even after reaching a full crystallinity in the MFI nanosheets through a kind of solution-mediated ripening process. The crystal ripening processes along the *b*-crystal axis (i.e., perpendicular to the nanosheet layer) appear to be prevented by the hydrophobic alkyl tails. The ripening processes may lead to an increase in the *a*−*c* plane area. The zeolite layers with wide *a*−*c* planes were more efficiently assembled in a multilamellar array through hydrophobic interactions between the surfactant tails outside the zeolite layers. The overall stacking number of zeolite nanosheets in the multilamellar array was typically 5−10 at 4 d. Longer heating increased the overall stacking number.

When ethanol was added to condition a, no interlayer structural order was detected by low-angle XRD (conditions b and c). When water glass was used as a silica source without ethanol (condition d), full zeolite crystallization to the ordered multilamellar structure took 6 d. The addition of 400 ethanol into this condition decreased the reaction time to 4 d (condition e). In this case, further heating resulted in a significant increase in the structural order similar to the case of a. When fumed silica (Aerosil) was used as a silica source, disordered nanosheets were obtained even with ethanol. In addition, a very small amount of bulk crystals (<5% in quantity, with an unknown structure) was detected by SEM. No transitions from the disordered structure to an ordered phase were observed during the heating experiment for 10 d.

The above results show that the formation of a multilamellar mesostructure is influenced by the amount of ethanol and the choice of silica source. The effect of the silica source is very common in zeolite synthesis, because the synthesis is accomplished through a delicate harmony between thermodynamic factors and kinetic parameters. The ethanol effect can be attributed to its role as an organic cosolvent that can change the structure of surfactant micelles by entering the palisade region.[22−25] The amount of ethanol should be optimized for facile formation of a well-ordered multilamellar mesostructure. An excessive amount of ethanol causes the nanosheets to form a disordered arrangement. This is similar to the effects of alcohols in the synthesis of silica-based noncrystalline mesostructures such as MCM-48[23,24] and KIT-6[25] using organic surfactants, whereas the surface curvature of the surfactant micelles is influenced by organic coadditives like ethanol and *n*-butanol. It is known that, at the beginning of hydrothermal treatment, micellar aggregates are formed in an aqueous solution and silicate anions are polymerized to form a liquid-crystal-like array (i.e., organic/inorganic composite).[22] Ethanol can promote the inorganic−organic assembly process and, at the same time, its reverse (dissolution) process by penetrating the micelle surface to the hydrophobic core during hydrothermal heating. In the present case of zeolite synthesis, crystal nucleation and growth processes of aluminosilicate gel can complicate the formation of multilamellar MFI structure nanosheets. The detailed mechanism is discussed in the following section. Note that only a small amount of ethanol promoted the organization of a multilamellar structure. It accelerated the crystal growth, perhaps by enhancing the surfactant mobility and via reassembly with zeolite nutrients.

It is reported that for the structure of the MCM-41-type, noncrystalline mesoporous silica can be changed by the addition

(21) Lund, K.; Muroyama, N.; Terasaki, O. *Microporous Mesoporous Mater.* **2009**, *128*, 71–77.
(22) Huo, Q.; Margolese, D. I.; Stucky, G. D. *Chem. Mater.* **1996**, *8*, 1147–1160.
(23) Gallis, K. W.; Landry, C. C. *Chem. Mater.* **1997**, *9*, 2035–2039.
(24) Kim, J. M.; Kim, S. K.; Ryoo, R. *Chem. Commun.* **1998**, 259–260.
(25) Kim, T.-W.; Kleitz, F.; Paul, B.; Ryoo, R. *J. Am. Chem. Soc.* **2005**, *127*, 7601–7610.

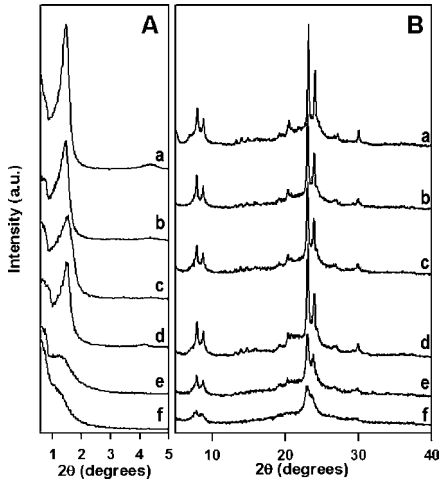

Figure 2. Low-angle (A) and high-angle (B) XRD patterns for as-synthesized MFI zeolite products, which were synthesized with $C_{22-6-6}Br_2$ under synthesis conditions a as given in Table 1, except for different Si/Al ratios. The Si/Al ratios in the zeolite samples of a−f are ∞, 134, 82, 49, 21, and 12, respectively. The Si/Al ratios in the gel compositions were ∞, 150, 100, 50, 25, and 15, respectively.

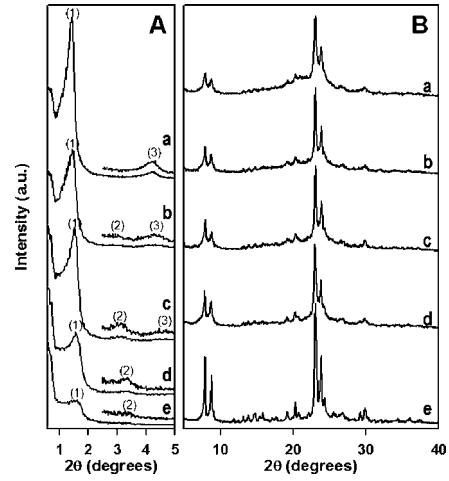

Figure 3. Low-angle (A) and high-angle (B) XRD patterns for as-synthesized MFI zeolite products, which were synthesized with (a) $C_{22-6-6}Br_2$, (b) $C_{20-6-6}Br_2$, (c) $C_{18-6-6}Br_2$, (d) $C_{16-6-6}Br_2$, and (e) $C_{12-6-3}Br_2$ as the SDA, respectively. All synthesis conditions are the same as condition a in Table 1, except for the different SDAs. The low-angle XRD patterns show that the interlayer spacing could be controlled by the SDAs.

of organic additives or by using surfactants with different micelle packing parameters. Organic additives are known to affect the packing parameter of the surfactant by changing the volume or radii of hydrophobic or hydrophilic parts, leading to a structural change in the mesoporous silica.[22] For example, the addition of a large amount of ethanol changed the structure from cubic to vesicular or lamellar mesophase.[22,23] We applied these techniques in an effort to obtain other nanomorphous MFI zeolites (e.g., cubic or hexagonal) aside from the ordered multilamellar assembly of nanosheets or their disordered unilamellar assembly. However, our attempts using ethanol, *n*-butanol, and 1,3,5-trimethylbenzene have proven unsuccessful thus far. We obtained a hexagonal mesostructure similar to MCM-41 before zeolite crystallization started, but the structure changed to 2D nanosheets upon crystallization. Thus, the almost 2D-like crystal growth tendency of MFI was a dominant factor over the control of the surfactant packing parameters. For the crystalline framework of a zeolite, it would be much more difficult to conform the surface curvature of a surfactant micelle than in the case of noncrystalline silica frameworks in the MCM-41-type mesoporous materials. Nanomorphous structures composed of ordered mesopores would be easier to synthesize with BEA zeolite than with MFI, whereas framework curvatures might be generated relatively easily in BEA owing to the intergrowth of several crystal polymorphs.

Figure 2 shows XRD patterns for MFI zeolite samples, which were synthesized with $C_{22-6-6}Br_2$ under the same synthesis condition as a in Table 1 except for the Al content. The Si/Al ratio in the reaction mixture was varied over a range from 15 to ∞. The Si/Al ratios for the resultant zeolite products were about 15% lower than the ratios for the gel compositions, as noted in the figure caption. As shown in Figure 2, the low-angle XRD peaks decreased in intensity as the Al content in zeolite increased. This indicates a loss of multilamellar ordering due to Al. Well-ordered multilamellar MFI zeolites were obtained with the Si/Al ratios between 30 and ∞ in the gel composition. At higher Al content beyond Si/Al = 30, the poorly ordered arrangements of zeolite nanosheets were obtained. In addition, the high-angle XRD peaks became broader, indicating that the coherent crystal domains decreased in size as the Al content was increased. The zeolite formation was also significantly retarded with high Al content. The XRD peak broadening and the decelerated crystallization rate agree with previous reports on the synthesis of high-silica BEA and MFI zeolites.[26−28] For previous works on bulk zeolites, it was reported that final crystal sizes decreased as Al content in the starting gel composition was increased. The Al content had significant effects on the final morphology and the crystal appearance. Well-faceted zeolite crystals were obtained in the case of low Al content, whereas small nanoparticles were obtained with high Al content. Similarly, we confirmed by SEM that the diameter of the $a-c$ plane decreased, and the arrangement of the MFI nanosheets became disordered as the Al content was increased (SEM images not shown here). However, we have not investigated whether the Al atoms are located inside the nanosheets or as a nonframework Al. A more specific study using solid-state NMR technique would be necessary to investigate the location of Al.

Control of Interlamellar Spacings by SDA. The interlayer spacings could be controlled by using SDAs with different hydrophobic tails. As shown in Figure 3A, the first-order reflection corresponding to multilamellar MFI zeolite nanosheets gradually shifted to a larger 2θ value as the chain length decreased. The MFI zeolite synthesized with $C_{22-6-6}Br_2$ (i.e., for C_{22}-MFI) exhibited a first-order reflection at $2\theta = 1.45°$ ($d_{(1)} = 6.1$ nm). C_{20}-MFI, C_{18}-MFI, C_{16}-MFI and C_{12}-MFI showed gradual shifts to 1.50° ($d_{(1)} = 5.9$ nm), 1.54° ($d_{(1)} = 5.7$ nm), 1.60° ($d_{(1)} = 5.5$ nm), and 1.70° ($d_{(1)} = 5.2$ nm), respectively. In the case of C_{12}-MFI, a C_3-alkyl group was bonded instead of C_6 at the headgroup of SDA, thus providing hydrophilic−hydrophobic balance between the headgroup and the short tail in the C_{12}−SDA. C_6-alkyl groups were bonded in C_{16} to C_{22}−SDAs. The synthesis result presented in Figure 3 indicates that all the SDAs could generate ordered multilamellar MFI zeolite structures. Relatively low diffraction intensities can

(26) Tosheva, L.; Valtchev, V. P. *Chem. Mater.* **2005**, *17*, 2494–2513.
(27) Persson, A. E.; Schoeman, B. J.; Sterte, J.; Otterstedt, J.-E. *Zeolites* **1995**, *15*, 611–619.
(28) Camblor, M. A.; Corma, A.; Valencia, S. *Microporous Mesoporous Mater.* **1998**, *25*, 59–74.

Scheme 1. Schematic Representation of Phase Transformation Detected by XRD and TEM during the Hydrothermal Synthesis of Multilamellar MFI Zeolite Using $C_{22\text{-}6\text{-}6}Br_2$ and Its Pillaring Process

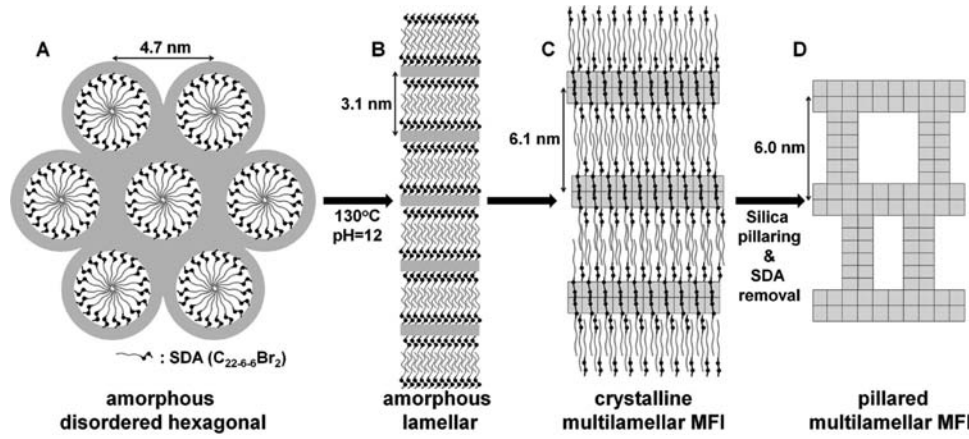

be seen in the XRD patterns as the hydrophobic tails became shorter in the SDAs. This change can be attributed to a decrease in the thickness of the surfactant layer while the thickness of the zeolite nanosheets remains constant. The accidental extinction of the second-order reflection did not appear in other C_n-MFI samples aside from C_{22}-MFI, due to the mismatch between the thickness of a single MFI nanosheet and one-half of the surfactant-layer thickness.

In addition to $C_{22-6-6}Br_2$, other C_{22}−SDAs with different head alkyl groups (i.e., $C_{22-6-0}Br$, $C_{22-6-3}Br_2$, and $C_{22-6-8}Br_2$) could be used as SDAs for the same multilamellar zeolite. However, the differences in these SDAs caused some changes in the multilamellar ordering and the time required for hydrothermal reaction. $C_{22-6-6}Br_2$ yielded the best structural order and the shortest time for synthesis. It was suggested in a previous study that the SDA head groups of two confronting surfactant molecules would be embedded in a straight channel along the *b*-crystal axis (Scheme 1C).[10] Our synthesis results support that C_6-alkyl groups could provide the optimum distance between two head groups for the formation of a zeolite nanosheet. In the case of $C_{22-6-8}Br_2$, the C_8-alkyl groups appeared to slightly exceed the optimum length. On the other hand, $C_{22-6-3}Br_2$ or $C_{22-6-0}Br$ seemed to provide a somewhat smaller headgroup for the nanosheet synthesis. This may explain why the other SDAs except $C_{22-6-6}Br_2$ required longer hydrothermal times for multilamellar organization. In addition, the multilamellar ordering resultant from these SDAs was somewhat lower than the synthesis result obtained with $C_{22-6-6}Br_2$.

Transformation from Noncrystalline Mesoporous Silica to Crystalline Zeolite Nanosheets during Hydrothermal Synthesis. The zeolite generation mechanism by $C_{22-6-6}Br_2$ was studied through the investigation of solid precipitates that could be collected at various times of the hydrothermal reaction. The synthesis temperature was chosen as 130 °C in order to sufficiently slow down the zeolite assembly process. The Al source was excluded for simplicity, and water glass was used as an inexpensive silica source without ethanol. The synthesis condition was the same as condition d in Table 1, except for the lower temperature. Precipitated sample aliquots were periodically taken from the synthesis mixture during heating at 130 °C. Figure 4 shows the XRD patterns of the samples collected during the period of 10 min−20 d. The XRD patterns, displayed with time, indicate that the initial gel (10 min) had a poorly ordered hexagonal mesostructure ($2\theta_{100} = 2.0°$, and $2\theta_{110} = 3.5°$) with an amorphous silicate framework. The initially

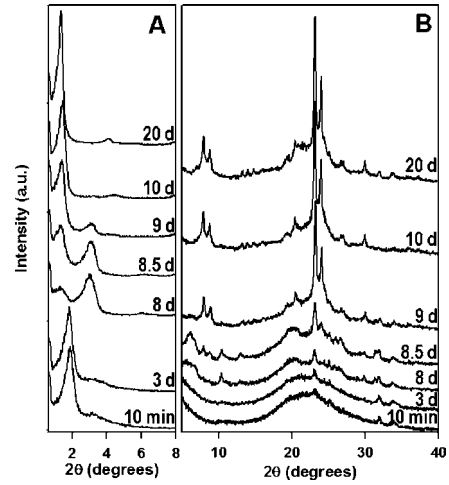

Figure 4. Low-angle (A) and high-angle (B) XRD patterns for the as-synthesized MFI zeolite products collected after various synthesis times with $C_{22-6-6}Br_2$, under the synthesis condition d given in Table 1, excluding the Al source.

hexagonal phase still remained for 7 d at 130 °C. This hexagonal phase disappeared as the hydrothermal reaction proceeded to 8 d, and a highly ordered lamellar phase was observed. Hence, the XRD peaks corresponding to the hexagonal peaks were replaced by well-resolved first-order ($2\theta = 2.9°$) and second-order ($2\theta = 5.8°$) reflections originating from the new multilamellar structure. The lamellar phase was still noncrystalline. The noncrystalline lamellar phase disappeared as the reaction was continued further (9 d), and another lamellar phase with a larger *d*-spacing (i.e., smaller 2θ value) appeared. This was the final zeolite product, that is, an ordered multilamellar nanosheets with $d_{(1)} = 6.1$ nm. At 10 d under the given synthesis conditions, all the noncrystalline phases were completely converted to crystalline zeolite phase (Scheme 1A−C). This product was stable during the investigation period (up to 20 d) under the synthesis conditions. No other phases including bulk zeolite were detected. The lamellar order increased during the extended heating period, although full crystallinity had already been attained at 10 d. The synthesis time could be decreased to 6 d at 150 °C. At higher temperatures (e.g., 170 °C), however, synthesis failed due to decomposition of the organic SDA.

Generally, for the formation of supramolecular assemblies between organic surfactants and silicate species, the kinetic packing parameter (*g*) is a key factor. The packing parameter

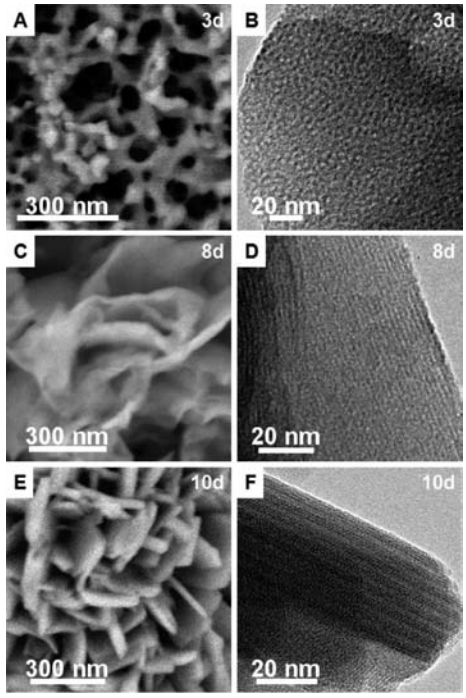

Figure 5. SEM (left column) and TEM (right column) images taken from samples collected at various reaction times (3, 8, and 10 d), during the formation of multilamellar MFI zeolite under the synthesis condition d given in Table 1. The images obtained at 3 d (A, B) show that an MCM-41-type mesoporous silica was initially formed without zeolite crystallinity. This silica transformed to an ordered lamellar mesophase (C, D), but there was still no zeolite crystallinity until 8 d. At 10 d (E, F), a fully crystalline, ordered multilamellar MFI zeolite phase was observed.

is defined as the ratio of the surfactant molecular volume (V) to the product of the effective headgroup area (a_0) and the effective surfactant length (l_c), given as follows: $g = V/a_0 l_c$.[22] Variation of surfactant packing can be the driving force for an initial mesophase and surfactant reassembly. Typical supramolecular templating action of $C_{22-6-6}Br_2$ having a bulky hydrophilic headgroup may yield a small g value between $^1/_3$ and $^1/_2$ at room temperature, which can result in spherical micelles with large surface curvature, i.e., hexagonal phase. However, at a suitably high temperature under a basic solution, the long hydrophobic tail (C_{22}) can increase the effective surfactant volume (V). Accordingly, due to the large g value, the hexagonal assembly appears to transform to an intermediate lamellar mesophase with low surface curvature (Scheme 1A,B). Since the diquaternary ammonium headgroup can strongly attract silicate species in their composites, the phase transformation seems to occur very slowly (after 8 d) compared to the case of monoammonium surfactant.[22]

SEM and TEM images in Figure 5 are consistent with the stepwise product changes noted above. The initial phase (A, B) shows a poorly ordered hexagonal mesostructure with spongelike macroporous morphologies. The intermediate lamellar phase (C, D) shows lettuce-leaf-like morphologies, which are typical of lamellar mesostructures without framework crystallinity such as MCM-50. The final product (E, F) shows thin crystal-like morphologies. It would be interesting to determine whether the zeolite nanosheets are generated from the intermediate lamellar phase via a solid-state or solution-mediated transformation.[2] However, the present data are not sufficient for clarification of the transformation mechanism.

Pillaring of Multilamellar MFI Nanosheets. The multilamellar MFI zeolite for pillaring was prepared by following condition a in Table 1. Figure 6 shows high-resolution SEM and TEM images of the pillared sample (P-C_{22}-MFI). The images were obtained after calcination of the pillared sample. Both images show that the zeolite nanosheets were well-supported by silica pillars, forming an ordered multilamellar architecture. The silica pillars can retain interlayer mesoporosity even after SDA removal. Remarkably, the silica pillars are clearly visible in the SEM image (white arrows in Figure 6A). This is the first reported observation of pillars by SEM among pillared clays and zeolites, to the best of our knowledge. Some pillars could also be identified in the TEM images despite their irregular positioning on the $a-c$ plane of the zeolite structure (white arrows in Figure 6B). In addition, it is clearly observable that several zeolite nanosheets of a single-unit-cell thickness are parallel to each other, retaining a fully ordered assembly of zeolite nanosheets with a vertical diameter of 3.9 nm.

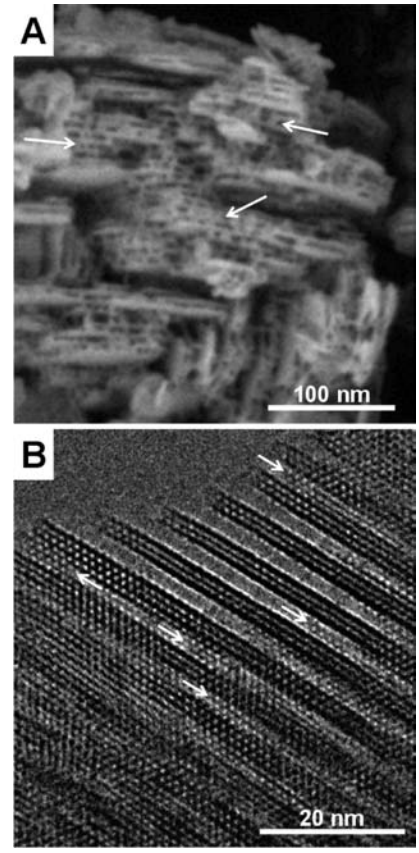

Figure 6. High-resolution SEM (A) and TEM (B) images of the ordered multilamellar MFI zeolite nanosheet synthesized with $C_{22-6-6}Br_2$, in which the interlayer spacing has been supported with silica pillars. These images were taken after calcination. White arrows in parts A and B indicate the silica pillars between the zeolite nanosheets.

Figure 7 shows the XRD patterns of the C_{22}-MFI sample, which were taken in three differently treated states: as synthesized with Si/Al = 49, after calcination without pillaring, and after calcination with pillaring. The first-order reflection for the calcined P-C_{22}-MFI in the presence of silica pillars is observed at $2\theta = 1.45°$ ($d_{(1)} = 6.1$ nm). As discussed above, the absence of the second-order reflection is due to an accidental extinction.[21] The presence of the third-order reflection indicates that the long-range structural order is fully retained in the C_{22}-MFI sample. Even the fourth-order reflection could be observed when a pure-silica sample was pillared (Supporting Information, Figure S4). Considering the single-unit-cell thickness of an individual MFI layer, the interlayer spacing of the P-C_{22}-MFI sample is

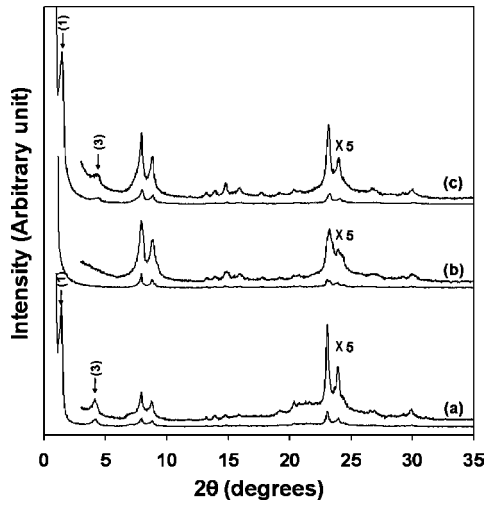

Figure 7. XRD patterns for the C_{22}-MFI sample, taken in three differently treated states: as synthesized with Si/Al = 49 (a), after calcination without pillaring (b), and after calcination with pillaring (c). Magnified XRD patterns are also presented for each pattern.

calculated to be 4.1 nm, which is consistent with the value determined by TEM (3.9 nm). The mesopore vertical diameter changed from 4.1 to 3.4 nm when the C_{22}-alkyl tail was replaced by a shorter C_{16} (Supporting Information, Figures S2 and S3). This suggests that the mesopore diameter could be controlled over a wider range than 3.4−4.1 nm, if a short alkyl chain or a pore expanding agent is used.

The pore structures of the P-C_{22}-MFI and C_{22}-MFI are compared on the basis of Ar adsorption. The results were compared by using nonlocal density functional theory (NLDFT) to analyze the Ar adsorption isotherms (see also Supporting Information, Figure S1). Figure 8 shows the cumulative pore volume and pore size distributions for P-C_{22}-MFI and C_{22}-MFI samples after calcination. The distributions were calculated from NLDFT assuming a cylindrical pore model. Both samples exhibit a very sharp peak centered at 0.55 nm. This is in agreement with the micropore dimension of the MFI framework. A steep increase of the cumulative pore volume in a pore size range between 3.0 and 5.0 nm is observed in the P-C_{22}-MFI sample. This indicates that the P-C_{22}-MFI possesses uniform mesopores (see also Supporting Information, Figure S1), while the C_{22}-MFI after calcination without silica pillaring exhibited a much broader pore size distribution. The uniformity of mesopores is comparable to that of ordered mesoporous silica materials like MCM-41. The pillared zeolite exhibits a high BET surface area (615 m^2/g) and a large pore volume (0.44 mL/g) due to the preservation of an ordered multilamellar structure.

Interestingly, the silica pillars were highly likely to be crystallized into a part of the MFI zeolite during the pillaring process. The first clue of this is the TEM image in Figure 6B, which shows micropores inside the silica pillars (white arrows). Due to their irregular positioning on the $a-c$ plane of the zeolite structure, the silica pillars were not easily observable in TEM images. The second is that no significant lattice contraction was detected by XRD when the sample was calcined after pillaring. Normally, a lattice contraction of more than 10% can be easily detected by XRD when a mesoporous silica material with a noncrystalline framework is calcined. However, no such contraction was detected in the case of the P-C_{22}-MFI sample. The third is in the micropore analysis by Ar adsorption. According to the ICP analysis, the Si/Al ratio in the zeolite phase was

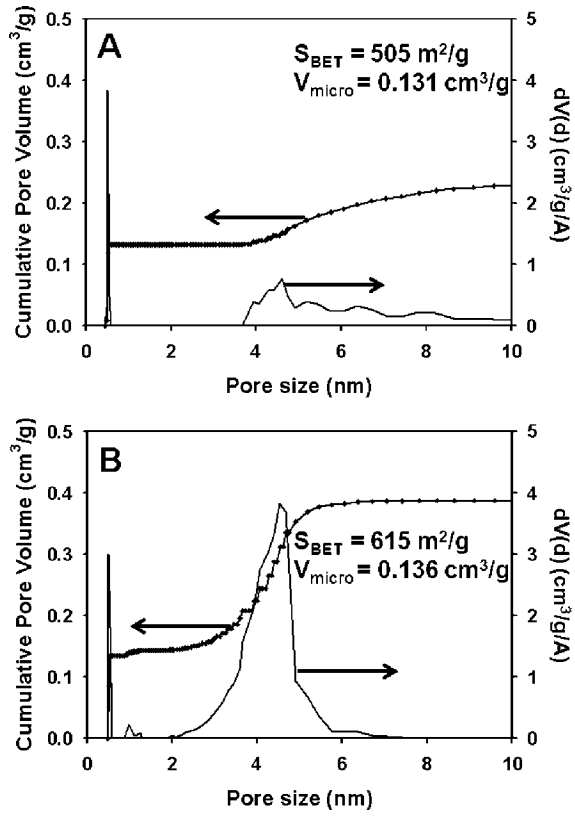

Figure 8. Cumulative pore volume and pore size distributions for the C_{22}-MFI (A) and P-C_{22}-MFI (B). S_{BET} is the BET surface area (m^2/g) and V_{micro} is the micropore volume (cm^3/g).

increased from 49 to 57. This is due to the additional silica content increased by silica pillars. Furthermore, there was no significant amount of Al or Si leaching into the solution phase during the pillaring process. On the basis of the ICP analysis, the absolute amount of silica in the zeolite phase was increased by 14 wt % due to the silica pillaring.

Despite the 14 wt % increase in the sample mass, we detected no significant change in the micropore diameters or volume. As shown in Figure 8B, the cumulative micropore volume for a P-C_{22}-MFI sample with up to 2-nm diameter was 0.136 cm^3/g. This is nearly the same as the micropore volume (0.131 cm^3/g) of the calcined zeolite without pillaring (C_{22}-MFI). There was a slight increase in the micropore volume around 1 nm after pillaring, but the change was negligible as compared to the 14 wt % mass change. With the three clues discussed so far, we suggest that the silica pillars could have a crystalline microporous structure corresponding with that of MFI zeolite. As reported by Choi et al.,[10] one-half of the surfactant could be extracted from the as-synthesized MFI zeolite. These surfactant molecules were located in the surfactant micelles as "dummy fillers", while the other half acted as the zeolite SDA (Scheme 1C). The microporous structure of the pillars could be generated due to the MFI structure-directing ability of the quaternary ammonium groups in the dummy filler surfactant molecules, during the pillaring process including hydrolysis at 90 °C.

Silica leaching from zeolite in the pillaring process was reported with layered zeolite precursors like MWW and FER.[11,14−17] This was likely due to a preswelling step using a highly basic aqueous solution of tertrapropylammonium hydroxide in the presence of cetyltrimethylammonium bromide.[11,14−17]

The pH of the swelling solution is 13, which is sufficiently basic for silica dissolution. In our study, the layer-by-layer swelling treatment under the strongly basic condition was unnecessary because the MFI zeolite was already synthesized in the multilamellar mesostructure. Therefore, the as-synthesized MFI zeolite was treated with neat TEOS liquid and subsequently hydrolyzed by distilled water. The pH of the aqueous solution was between 8 and 9 after the hydrolysis was finished. This accounts for the undetectable silica leaching in our work.

The amount of total acid sites in the P-C_{22}-MFI (Si/Al = 57) and its acid strength have been investigated by a temperature-programmed desorption of NH_3. The results indicate that the P-C_{22}-MFI contains both strong and weak acid sites, whereas the Al-MCM-41 shows only weak acid sites (Supporting Information, Figure S8 and Table S2). The presence of both kinds of acid sites in the P-C_{22}-MFI closely corresponds to the acidity of the conv-MFI zeolite. The acidity at the external surface has been analyzed with IR spectroscopy after adsorption of bulky amine (2,6-di-*tert*-butylpyridine) molecules that cannot be accommodated inside MFI micropores.[20] The results revealed that the P-C_{22}-MFI exhibits a 3-fold larger amount of external acid sites (per gram of zeolite), as compared to a conv-zeolite having much less external surface area (Supporting Information, Figure S9). Much more external acid sites could be expected if the surfaces of every MFI nanosheet had a similar acid concentration as the bulk zeolite surfaces. Indeed, the C_{22}-MFI sample which was not pillared exhibited greater amounts of external acid sites than P-C_{22}-MFI sample. This indicates that many of the surface Al sites could be covered by the reaction with the silica source during the treatments for pillaring. However, the P-C_{22}-MFI still retained a considerable amount of external acid sites as compared to the conv-MFI. In addition, facile accessibility to the zeolite micropores from all directions would allow the bulky molecules to be accommodated efficiently. Since the MFI framework possesses 3D pore connectivity along the whole crystal axis, the present materials would provide high molecular diffusion efficiency.

Conclusion

An ordered multilamellar assembly of MFI zeolite nanosheets was fully retained by silica pillaring between the adjacent 2-nm-thick layers. This is the first ordered material with 3D-structured zeolite framework. The pillared zeolite possesses many attractive features, such as long-range structural order in both micro- and mesopore regimes, whereby high surface area with large pore volume, large amount of external acid sites, and tunable interlayer meso-spacings according to the different hydrophobic tail length of surfactants are acquired. Besides, the wide planes of the nanosheets correspond to the (010) surface of the MFI zeolite structure, which are penetrated by straight 10-membered-ring channels (0.53 nm × 0.56 nm). Hence, the hierarchically ordered zeolites are expected to provide an extremely short diffusion path length during catalytic applications which accommodate bulky molecular species. In addition, the mesopores can offer a new site to support transition metal nanoparticles, in addition to the zeolite structural micropores. Another significant aspect of this pillared zeolite is that the mesopore walls (i.e., the external surface of the zeolite nanosheets) are terminated by numerous silanol (−Si−OH) groups. The surface could be functionalized at a considerably high density via a silylation process in order to modify the surface property (e.g., hydrophilic or hydrophobic property) or to graft a new catalytic active functional group.[29] The amount of organic groups (e.g., 3-aminopropyltriethoxysilane) grafted on the mesopore walls in this manner was about 1.1 mmol/g. Thus, pillared zeolites with various structures, such as the present MFI zeolite as well as previously reported MWW and FER zeolites,[11,14−17] present many new opportunities as a class of zeolitic materials having hierarchically ordered micro- and mesoporosity. Furthermore, the synthesis strategy using the zeolite-SDA-functionalized surfactant, detailed synthesis study, and characterization may be applied to new design of other nanomorphous zeolites with hierarchically ordered structure.

Acknowledgment. This work was supported by the National Honor Scientist Program of the Ministry of Education, Science and Technology in Korea. Electron microscopic studies were performed at the Electron Microscopy Center (EMC) at Stockholm University through support from the Knut and Alice Wallenberg Foundation.

Supporting Information Available: XRD, SEM, TEM, Ar adsorption, NH_3-TPD, and IR analyses. This material is available free of charge via the Internet at http://pubs.acs.org.

JA908382N

(29) Lee, D.-H.; Choi, M.; Yu, B.-W.; Ryoo, R. *Chem. Commun.* **2009**, *1*, 74–76.